Title: Inverse FEM for Full-Field Reconstruction of Elastic Deformations in Shear Deformable Plates and Shells

Authors: Alexander Tessler
Jan L. Spangler

ABSTRACT

The inverse problem of real-time reconstruction of full-field structural displacements is addressed through the application of a new variational formulation leading to versatile, robust and computationally efficient inverse shell finite element analysis. Utilizing surface strain measurements from strain sensors mounted on the load-carrying structural components, the methodology enables accurate computations of the three-dimensional displacement field. This high fidelity computational technology is essential for providing feedback to the actuation and control systems of the next generation of aerospace vehicles.

INTRODUCTION

Real-time reconstruction of full-field structural displacements is seen as enabling technology for providing feedback to the actuation and control systems of the next generation of aerospace vehicles with morphed-wing architecture. To facilitate such capabilities, load-carrying structural members will be instrumented with a network of strain sensors, e.g., fiber optic sensors with Bragg gratings.

Reconstruction of a displacement vector at every material point of the structure from a set of discrete strain measurements constitutes an inverse mathematical problem. Inverse problems are ill posed in the sense that they do not necessarily satisfy conditions of existence, uniqueness, and stability. For this class of mathematical problems that use experimentally measured data known only approximately and containing random error, Tikhonov and Arsenin [1] formulated a general method for constructing approximate solutions that are stable under small changes in the measured data. Their approach is based upon the fundamental concept of a regularizing operator. Recently, Shkarayev et al. [2-3], Bogert et al. [4], and Tessler and Spangler [5], using different least-squares approaches, focused

---

Alexander Tessler, NASA Langley Research Center, Hampton, Virginia 23681, U.S.A. Alexander.Tessler-1.@nasa.gov
Jan L. Spangler, Lockheed Martin Aeronautics Company, NASA Langley Research Center, Hampton, Virginia 23681, U.S.A.

on the inverse problem of reconstructing the three-dimensional displacements in plate and shell aerospace structures from in-situ strain-sensor measurements.

This paper presents an *inverse* finite element method (iFEM) based on the Tessler-Spangler [5] least-squares variational formulation. The error functional uses the least-squares-difference terms comprised of the Mindlin-theory strain measures that are expressed in terms of the displacements and the corresponding strain measures computed from the experimental strains. A penalty-parameter controlled regularization term enforces appropriate constraint conditions on the transverse shear strains. By virtue of these assumptions, all strain compatibility relations are explicitly satisfied. The inverse formulation does not use elastic or inertial material properties.

A three-node, inverse-shell element is developed having six conventional degrees-of-freedom at each node, i.e., three displacements and three rotations. The kinematic variables are interpolated using the lowest-order anisoparametric C^0-continuous functions, i.e., linear in-plane displacements and bending rotations, and a constrained-type quadratic deflection. These functions were adopted from an earlier Mindlin shell element formulation [6-7].

A computational example is presented for a statically loaded cantilevered plate for which experimentally measured strains have been obtained in a structures laboratory. Application of iFEM is demonstrated on this problem, and comparisons with the measured deflections and those obtained using the direct FEM are discussed.

THEORETICAL FOUNDATION

The deformations of an inverse, three-node flat shell element, herein denoted as iMIN3, are fully defined by the three components of the displacement vector, in accordance with Mindlin theory (refer to Figure 1):

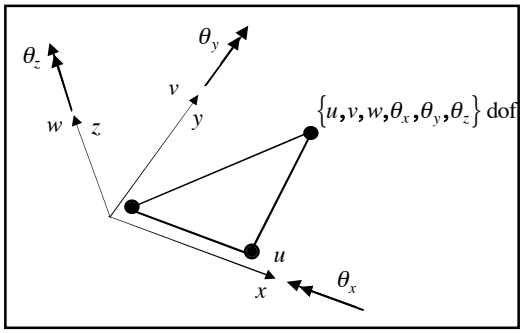

Figure 1. Three-node, inverse shell element, iMIN3.

$$u_x(x,y,z) = u + z\,\theta_y, \quad u_y(x,y,z) = v + z\,\theta_x, \quad u_z(x,y,z) = w \tag{1}$$

where $u = u(x,y)$ and $v = v(x,y)$ are the mid-plane displacements in the x and y directions, respectively; $\theta_x = \theta_x(x,y)$ and $\theta_y = \theta_y(x,y)$ are the rotations of the normal about the negative x and positive y axes, respectively; and $w = w(x,y)$ is the deflection variable which is constant across the thickness coordinate $z \in [-t,t]$, with $2t$ denoting the total shell thickness.

The strain-displacement relations, taking into account Equations (1), have the form

$$\begin{Bmatrix} \varepsilon_{xx} \\ \varepsilon_{yy} \\ \gamma_{xy} \end{Bmatrix} = \begin{Bmatrix} \varepsilon_{x0} \\ \varepsilon_{y0} \\ \gamma_{xy0} \end{Bmatrix} + z \begin{Bmatrix} \kappa_{x0} \\ \kappa_{y0} \\ \kappa_{xy0} \end{Bmatrix} \equiv \mathbf{e}(\mathbf{u}) + z\,\mathbf{k}(\mathbf{u}) \tag{2}$$

where the membrane strain measures associated with the stretching of the middle surface are given as

$$\mathbf{e}(\mathbf{u}) \equiv \begin{Bmatrix} \varepsilon_{x0} \\ \varepsilon_{y0} \\ \gamma_{xy0} \end{Bmatrix} = \begin{bmatrix} \frac{\partial}{\partial x} & 0 & 0 & 0 & 0 \\ 0 & \frac{\partial}{\partial y} & 0 & 0 & 0 \\ \frac{\partial}{\partial y} & \frac{\partial}{\partial x} & 0 & 0 & 0 \end{bmatrix} \begin{Bmatrix} u \\ v \\ w \\ \theta_x \\ \theta_y \end{Bmatrix} \equiv \mathbf{L}^m\,\mathbf{u} \tag{3}$$

In addition, the bending curvatures are

$$\mathbf{k}(\mathbf{u}) \equiv \begin{Bmatrix} \kappa_{x0} \\ \kappa_{y0} \\ \kappa_{xy0} \end{Bmatrix} = \begin{bmatrix} 0 & 0 & 0 & 0 & \frac{\partial}{\partial x} \\ 0 & 0 & 0 & \frac{\partial}{\partial y} & 0 \\ 0 & 0 & 0 & \frac{\partial}{\partial x} & \frac{\partial}{\partial y} \end{bmatrix} \begin{Bmatrix} u \\ v \\ w \\ \theta_x \\ \theta_y \end{Bmatrix} \equiv \mathbf{L}^b\,\mathbf{u} \tag{4}$$

The transverse shear strains can also be expressed in terms of the same five kinematic variables as

$$\mathbf{g}(\mathbf{u}) \equiv \begin{Bmatrix} \gamma_{xz0} \\ \gamma_{yz0} \end{Bmatrix} = \begin{bmatrix} 0 & 0 & \frac{\partial}{\partial x} & 0 & 1 \\ 0 & 0 & \frac{\partial}{\partial y} & 1 & 0 \end{bmatrix} \begin{Bmatrix} u \\ v \\ w \\ \theta_x \\ \theta_y \end{Bmatrix} \equiv \mathbf{L}^s\,\mathbf{u} \tag{5}$$

Assuming the structure is instrumented with strain sensors (e.g., conventional strain rosettes or fiber-optic Bragg-grating sensors), strains are measured at the locations $\mathbf{x}_i = (x_i, y_i, \pm t)$ representing the top and bottom shell surfaces (refer to Figure 2). Evaluating Equations (2) at these discrete locations, the relationships between the measured surface strains and the reference plane strains and curvatures can be readily established as

$$\mathbf{e}_i^{\varepsilon} \equiv \begin{Bmatrix} \varepsilon_{x0}^{\varepsilon} \\ \varepsilon_{y0}^{\varepsilon} \\ \gamma_{xy0}^{\varepsilon} \end{Bmatrix}_i = \frac{1}{2}\left(\begin{Bmatrix} \varepsilon_{xx}^{+} \\ \varepsilon_{yy}^{+} \\ \gamma_{xy}^{+} \end{Bmatrix}_i + \begin{Bmatrix} \varepsilon_{xx}^{-} \\ \varepsilon_{yy}^{-} \\ \gamma_{xy}^{-} \end{Bmatrix}_i \right) \tag{6}$$

$$\mathbf{k}_i^{\varepsilon} \equiv \begin{Bmatrix} \kappa_{x0}^{\varepsilon} \\ \kappa_{y0}^{\varepsilon} \\ \kappa_{xy0}^{\varepsilon} \end{Bmatrix}_i = \frac{1}{2t}\left(\begin{Bmatrix} \varepsilon_{xx}^{+} \\ \varepsilon_{yy}^{+} \\ \gamma_{xy}^{+} \end{Bmatrix}_i - \begin{Bmatrix} \varepsilon_{xx}^{-} \\ \varepsilon_{yy}^{-} \\ \gamma_{xy}^{-} \end{Bmatrix}_i \right) \tag{7}$$

In the above equations, the ε superscript is used to signify the existence of experimental error in the strain measurements and, hence, in $\mathbf{e}_i^{\varepsilon}$ and $\mathbf{k}_i^{\varepsilon}$.

THREE-NODE, INVERSE SHELL ELEMENT

Using the above stated assumptions, a simple and versatile *inverse shell element* is developed consisting of three nodes and six engineering degrees-of-freedom (dof) at each node, as illustrated in Figure 1. To avoid singular numerical solutions in shell models, a drilling rotation, θ_z, degree-of-freedom is added using the *artificial stiffness* approach [7].

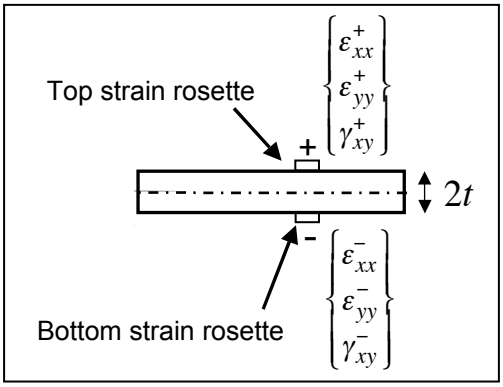

Figure 2. Shell surfaces instrumented with strain rosettes.

The element matrices are derived from a least squares smoothing functional [5], for which an extremum is sought for a fixed value of a scalar penalty parameter $\lambda > 0$. For an inverse shell finite element of area A_e, this functional can be expressed as

$$\Phi_e^{\lambda}(\mathbf{u}) = \left\| \mathbf{e}(\mathbf{u}) - \mathbf{e}^{\varepsilon} \right\|^2 + \left\| \mathbf{k}(\mathbf{u}) - \mathbf{k}^{\varepsilon} \right\|^2 + \lambda \left\| \mathbf{g}(\mathbf{u}) - \mathbf{g}^{\varepsilon} \right\|^2 \tag{8}$$

In Equation (8), the squared norms are given as,

$$\begin{aligned} \left\| \mathbf{e}(\mathbf{u}) - \mathbf{e}^{\varepsilon} \right\|^2 &\equiv \frac{1}{n} \int_{A_e} \sum_{i=1}^{n} \left[\mathbf{e}(\mathbf{u})_i - \mathbf{e}_i^{\varepsilon} \right]^2 d\mathrm{x}\, d\mathrm{y} \\ \left\| \mathbf{k}(\mathbf{u}) - \mathbf{k}^{\varepsilon} \right\|^2 &\equiv \frac{(2t)^2}{n} \int_{A_e} \sum_{i=1}^{n} \left[\mathbf{k}(\mathbf{u})_i - \mathbf{k}_i^{\varepsilon} \right]^2 d\mathrm{x}\, d\mathrm{y} \\ \left\| \mathbf{g}(\mathbf{u}) - \mathbf{g}^{\varepsilon} \right\|^2 \equiv \frac{1}{n} \int_{A_e} \sum_{i=1}^{n} \left[\mathbf{g}(\mathbf{u})_i - \mathbf{g}_i^{\varepsilon} \right]^2 d\mathrm{x}\, d\mathrm{y} \quad &\text{or} \quad \left\| \mathbf{g}(\mathbf{u}) - \mathbf{g}^{\varepsilon} \right\|^2 \equiv \int_{A_e} \mathbf{g}(\mathbf{u})^2 d\mathrm{x}\, d\mathrm{y} \end{aligned} \tag{9}$$

where $n \geq 1$ is the number of strain sensor locations that fall within the element domain.

Note that the squared norms in Equations (9) differ slightly from those introduced in [5]. The main difference is that the curvature norm is normalized with respect to the squared shell thickness; whereas in [5] the shell reference area is used. The present curvature norm, with respect to the geometric parameters, is consistent with the bending strain energy corresponding to Mindlin theory.

In Equations (9), the second form of the transverse shear norm makes the formulation applicable only to thin (Kirchhoff-type) plate and shell structures that do not exhibit shear deformation; whereas the first form applies to moderately thick, shear-deformable structures. The transverse shear strains, however, cannot be directly obtained from the surface strains, and auxiliary procedures are required in order to determine these quantities (refer to [5] for further discussions of this issue). The transverse shear norm in Equation (8) is controlled by a small regularization parameter $\lambda > 0$ (the λ values in the range of 10^{-5}–10^{-8} yield consistent and stable performance), providing the appropriate coupling control between the bending and transverse shear terms.

Utilizing the displacement finite element method, the displacement field in Equation (8) is interpolated using a set of suitable shape functions,

$$\mathbf{u} = \mathbf{N}\mathbf{u}_e, \quad (\mathbf{u}_e^T = \{u_i, \quad v_i, \quad w_i, \quad \theta_{xi}, \quad \theta_{yi}\}, i = 1,2,3) \tag{10}$$

where $\mathbf{N}$ denotes a matrix of C^0-continuous *anisoparametric* shape functions. The kinematic variables are consistent with respect to the order of interpolation, where the deflection variable, w, is interpolated with a quadratic polynomial, and the other four variables vary linearly over the element (refer to [6-7] for further details on these interpolations). The resulting membrane strains and bending curvatures are constant,

and the transverse shear strains are linear, across the element. This implies that, for a given distribution of strain sensors, an *optimal* iFEM mesh would require the strain sensors be located at the element centroids.

Substituting Equation (10) into Equations (9), and minimizing Equation (8) with respect to the nodal displacement dof, results in the element matrix equation,

$$\mathbf{K}\,\mathbf{u}_e = \mathbf{f}_e \tag{11}$$

where, for brevity, the detailed expressions for $\mathbf{K}$ and $\mathbf{f}_e$ are omitted.

The element matrices of the discretized structure are then assembled into a linear system of equations, taking into account appropriate transformations of the displacement dof from the element to global system coordinates, and performing the standard finite element assembly operation. Mindlin-type displacement boundary conditions, corresponding to the problem definition, are then imposed, producing a nonsingular system matrix (refer to [5] for the discussion on the boundary conditions for the inverse formulation). The resulting solution for the displacement dof exists and is unique since the system matrix is nonsingular. Once the nodal displacements are obtained, a straightforward computation at the element level provides the results for the smoothed element strains, and with the use of material constitutive relations, the stresses are also readily computed. All of these computations are based on linear equations and therefore are computationally efficient.

CANTILEVERED PLATE IN BENDING

A cantilevered aluminum plate subjected to a static transverse force near the tip was tested in a structures laboratory [4]. The plate was also analyzed using the direct FEM plate bending analysis and the inverse FEM using a relatively coarse mesh of iMIN3 elements. The plate dimensions, loading, boundary conditions, material properties, and locations of the 28 strain rosettes, positioned on the bottom of the plate surface, are depicted in Figure 3. Also shown is a triangular mesh consisting of 28 iMIN3 elements. The mesh is such that at least one strain rosette falls within each element. The mesh extends up to the location of the applied force only, since the part of the plate to the right of the load is free of stress and need not be modeled.

To establish an accurate numerical solution, a direct FEM convergence study was carried out with three levels of progressively increasing mesh refinements, using meshes of triangular and quadrilateral elements. The most refined mesh consisted of 432 square, uniformly distributed elements, possessing 1400 dof. In the analyses, three different elements were employed: a three-node triangular element, MIN3, available in NASA's COMET-AR [8] code, a three-node triangular element, S3, and a reduced-integration quadrilateral shell element, S4R, both available in the ABAQUS [9] code. All element models converged rapidly to the deflection of approximately 0.27 inches. It is noted that even the low-fidelity mesh of MIN3 elements (the mesh is shown in Figure 3) produced adequate deflection results, with the error for the maximum deflection less than 1 percent. This observation suggests that the low-fidelity mesh can also be effective for the inverse analysis since iMIN3 has the same kinematic interpolations as MIN3.

In Figure 4, the deflection contours corresponding to the direct FEM analysis, using the high-fidelity mesh of S4R elements and the inverse FEM using the low-fidelity mesh of iMIN3 elements, are presented. In the inverse FEM solution, the actual strain measurements from the 28 rosettes were used. As depicted in the figure, the direct and inverse FEM results are found to be in excellent agreement across the entire plate domain including the maximum values.

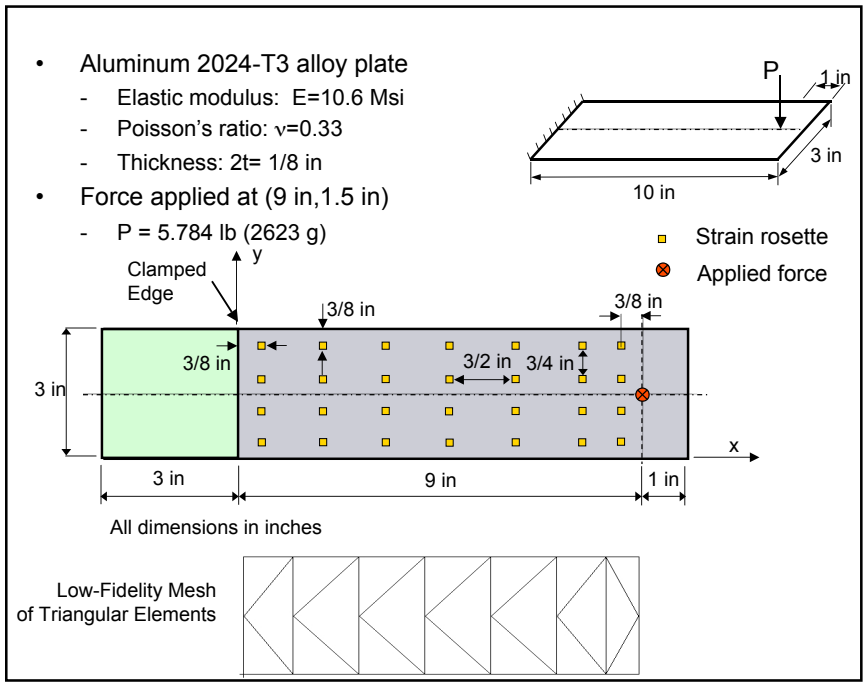

Figure 3. Cantilevered plate under transverse force.

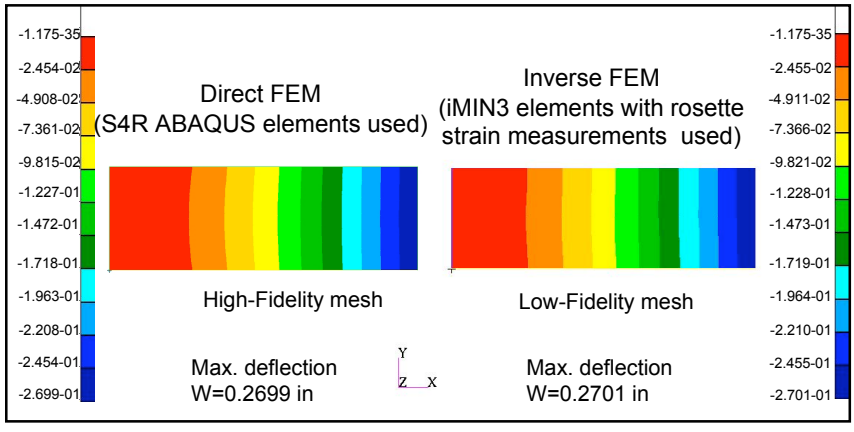

Figure 4. Deflection contours corresponding to direct FEM (high-fidelity mesh of S4R elements, ABAQUS [9]) and inverse FEM (low-fidelity mesh of iMIN3 elements, COMET-AR [8]).

CONCLUSIONS

In this paper, a novel *inverse* finite element method (iFEM) was developed for the inverse problem of reconstructing the full-field structural displacements from experimentally measured surface strains in plate and shell structures. Based on a least squares smoothing functional that employs the complete set of strain measures, a three-node *inverse shell element* was developed enabling accurate, robust, and computationally efficient high-fidelity deformation reconstruction solutions. The methodology explicitly enforces all strain compatibility relations and does not use elastic or inertial material properties. It is therefore applicable to both static and dynamic applications.

An example problem of a cantilevered plate was examined for which experimental measurements were obtained in a structures laboratory. Direct and inverse FEM solutions were obtained to validate the high accuracy predictions of deformations afforded through the inverse FEM modeling.

The methodology is seen as essential technology for providing real-time displacement feedback to the actuation and control systems of the next generation of aerospace vehicles, as well as for applications to airframe structural health-monitoring information systems.

REFERENCES

1. Tikhonov, V., and Arsenin, V. Y., 1977. "Solutions of Ill-Posed Problems," Winston, Washington, D.C.
2. Shkarayev, S., Krashantisa, R., and Tessler, A., 2001. "An Inverse Interpolation Method Utilizing In-Flight Strain Measurements for Determining Loads and Structural Response of Aerospace Vehicles," *Proceedings of Third International Workshop on Structural Health Monitoring*, Stanford, California, pp. 336-343.
3. Shkarayev, S., Raman, A., and Tessler, A., 2002. "Computational and Experimental Validation Enabling a Viable In-Flight Structural Health Monitoring Technology," *Proceedings of First European Workshop on Structural Health Monitoring*, Cachan (Paris), France, pp. 1145-1150.
4. Bogert, P. B., Haugse, E. D., and Gehrki, R. E., 2003. "Structural Shape Identification from Experimental Strains using a Modal Transformation Technique," *Proceedings of 44th AIAA/ASME/ASCE/AHS Structures. Structural Dynamics, and Materials Conference,* AIAA 2003-1626, Norfolk, Virginia.
5. Tessler, A. and Spangler, J. L., 2003. "A Variational Principle for Reconstruction of Elastic Deformations in Shear Deformable Plates and Shells," NASA/TM-2003-212445.
6. Tessler, A., and Hughes, T. J. R., 1985. "A Three-Node Mindlin Plate Element with Improved Transverse Shear," *Computer Methods in Applied Mechanics and Engineering*, Vol. 50, pp. 71-101.
7. Tessler, A, 1990. "A C^0-Anisoparametric Three-Node Shallow Shell Element," *Computer Methods in Applied Mechanics and Engineering*, Vol. 78, pp. 89-103.
8. Moas, E. (ed.) 1997. "COMET-AR User's Manual," NASA/CR-97-206284.
9. ABAQUS/Standard User's Manual, Version 6.3.1, Hibbitt, Karlsson, and Sorensen, Inc., Pawtucket, RI, 2002.